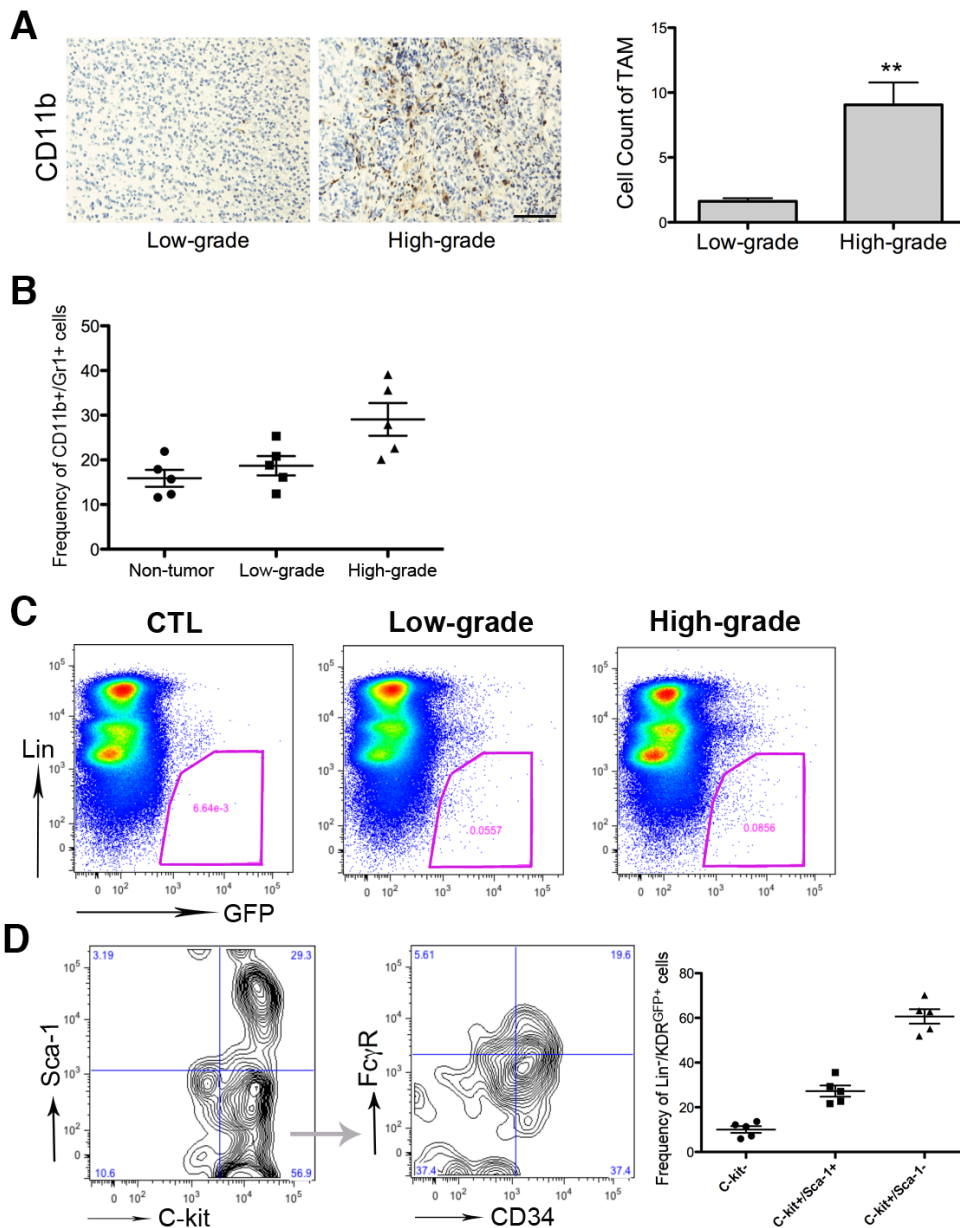


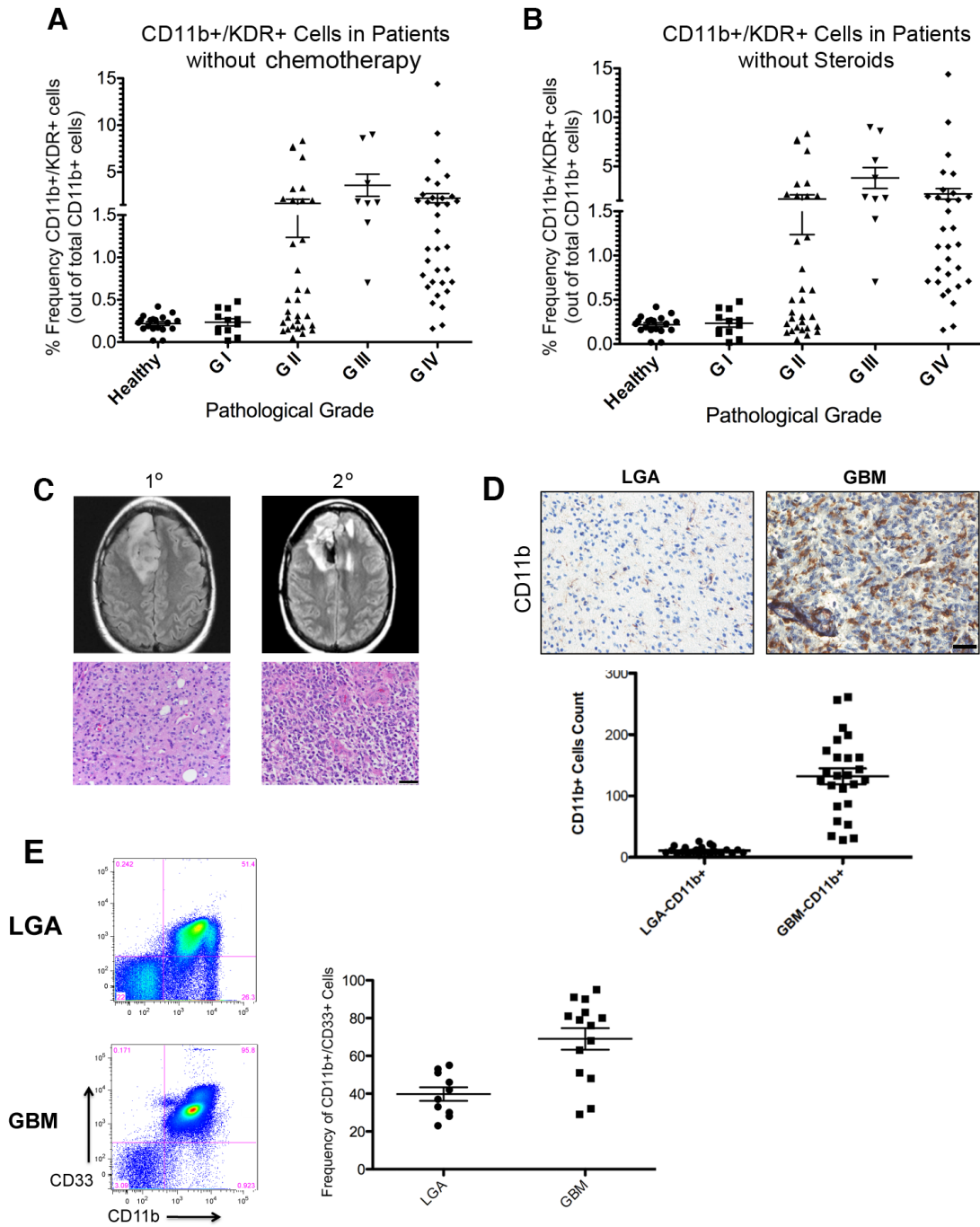
Supplementary Figure 1



Supplementary Figure 1. Characterization of myeloid cells in murine models. (A) IHC of CD11b on tumor tissue of PDGF-driven RCAS/*tva* gliomas at low-grade stages vs high-grade stages. Quantification of CD11b⁺ cells based on IHC images. Bar, 50 μ m, $n=10$, Means \pm SEM, $**P<0.01$ by student's t-test. (B) Frequency of CD11b⁺Gr1⁺ cells in peripheral blood of RCAS/*tva* tumor mice at low-grade stages vs high-grade stages. Means \pm SEM, $P<0.05$ by one way ANOVA. $n=5$. (C) Representative flow cytometry graphs of lineage markers (Lin) and GFP on myeloid cells from KDR^{GFP} mice bearing gliomas at low-grade and high-grade stages. Controls (CTL) are mice bearing the intact *KDR* locus without knocking in GFP. $n=5$. (D) Representative flow cytometry graphs of Sca-1 vs C-

kit within the Lin⁻KDR^{GFP+} population, and FcγR vs CD34 within the C-kit⁺Sca-1⁻ population. Frequency of C-kit⁻, C-kit⁺Sca-1⁺, C-kit⁺Sca-1⁻ cells within the Lin⁻KDR^{GFP+} population. *n*=5.

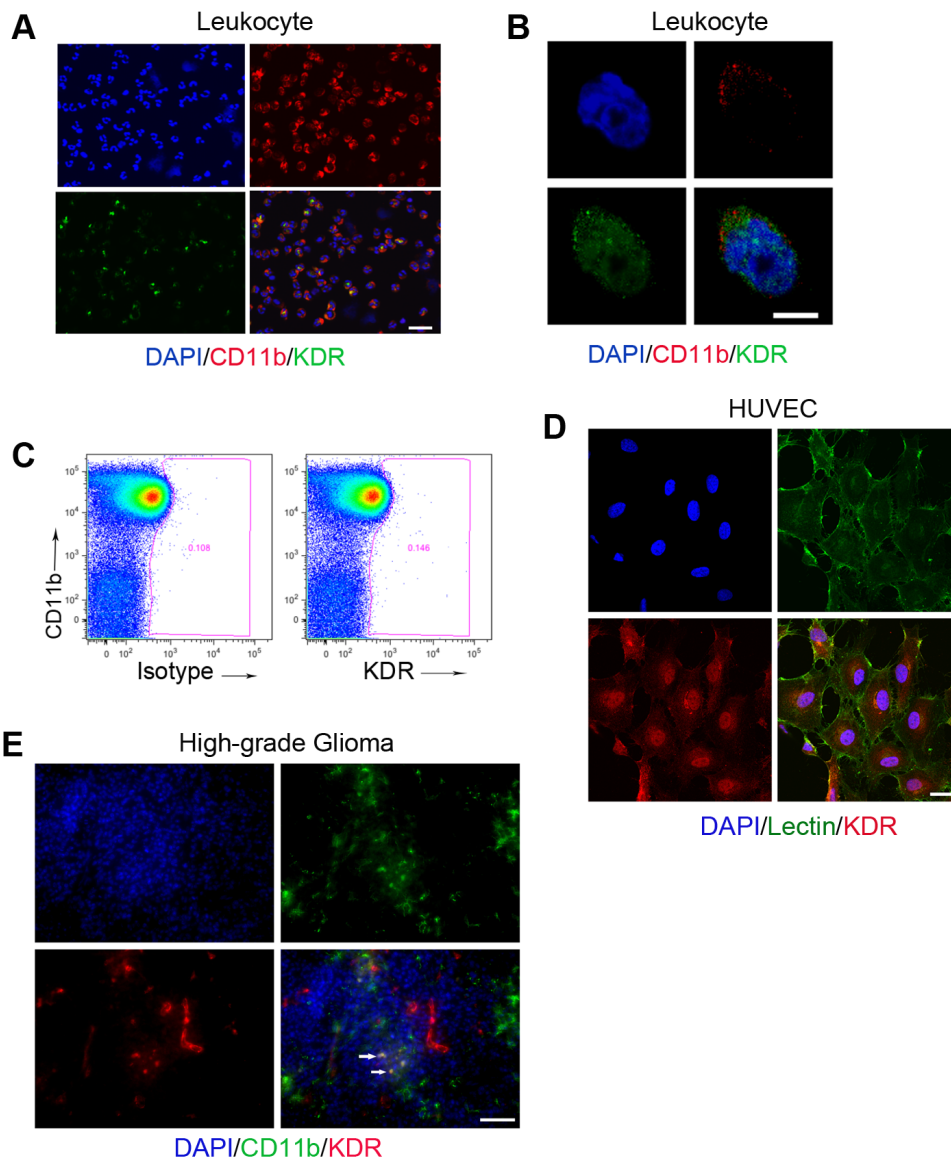
Supplementary Figure 2



Supplementary Figure 2. Characterization of myeloid cells in glioma patients. Dots-plot on frequency of CD11b⁺/KDR⁺ cells out of total CD11b⁺ cells in patients with different stages of glioma without chemotherapy $n=105$ (A), or without steroid treatment $n=104$ (B). Healthy donors served as controls. GIII/GIV vs healthy, one-way ANOVA, $P < 0.001$. (C) The initial (left) MRI and histology on a

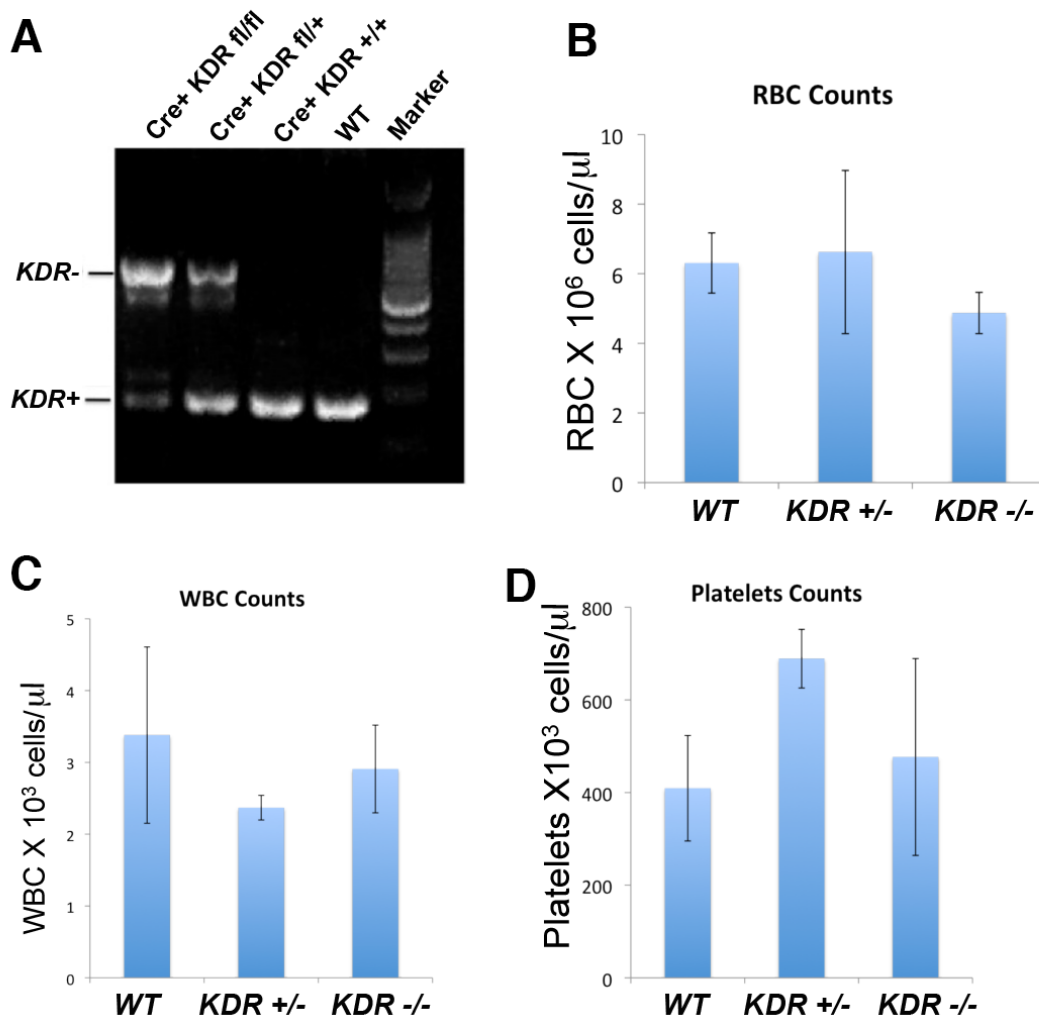
low-grade patient (Grade II), who showed high CD11b⁺KDR⁺ frequency in peripheral blood. Both MRI and histology (H&E) indicated the progression of diseases from primary low-grade tumor (1⁰) to secondary high-grade tumor (2⁰). Bar, 20 μ m. (D) IHC of CD11b on archived low-grade astrocytoma patients (Grade II) vs glioblastoma patients (Grade IV). Quantification of CD11b⁺ cells based on IHC images. Bar, 20 μ m, $n=20$, Means \pm SD, $P<0.001$ by Student's t-test. (E) Characterizing and quantification of MDSCs by flow cytometry in the periphery of low-grade astrocytoma patients (LGA, $n=10$) vs glioblastoma patients (GBM, $n=14$). Means \pm SD, $P<0.05$ by one-way ANOVA.

Supplementary Figure 3



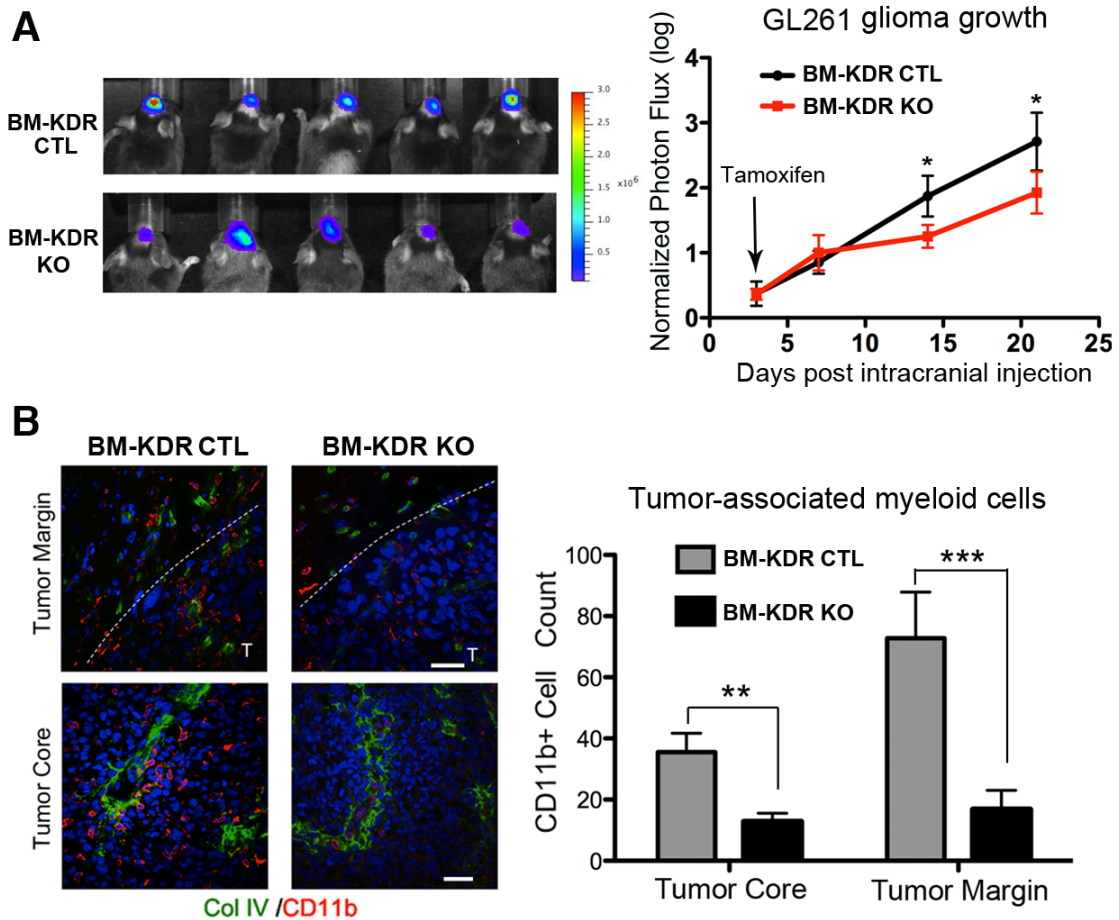
Supplementary Figure 3. Intracellular distribution of KDR in myeloid cells. (A) Immunofluorescence of KDR and CD11b on cytopinned white blood cells from glioblastoma patients. Nuclei were counterstained with DAPI. Bar, 10 μ m. *n*=3. (B) High-magnification immunofluorescence of KDR and CD11b acquired by confocal microscopy. Bar, 2 μ m. *n*=3. (C) Flow cytometry of CD11b, Isotype/KDR on non-permeabilized peripheral leukocytes in GBM patients. *n*=5. (D) Immunostaining of KDR and lectin (for cell membrane staining) on HUVECs. Bar, 10 μ m. *n*=3. (E) Costaining of KDR and CD11b on PDGF-driven high-grade murine glioma tissue. Bar, 50 μ m. *n*=5.

Supplementary Figure 4



Supplementary Figure 4. Validating the depletion of the *KDR* allele in bone marrow cells. (A) Amplification of the *KDR*⁺ or *KDR*⁻ allele on bone marrow cells of mice with indicated genetic backgrounds. Tamoxifen was applied to mice one week before testing. *n*=5. Complete bloods count on mice with WT, *KDR*^{+/-}, or *KDR*^{-/-} bone marrow; (B) red blood cells (RBCs); (C) white blood cells (WBCs); and (D) platelets. Means \pm SD, *P*>0.05 by one-way ANOVA.

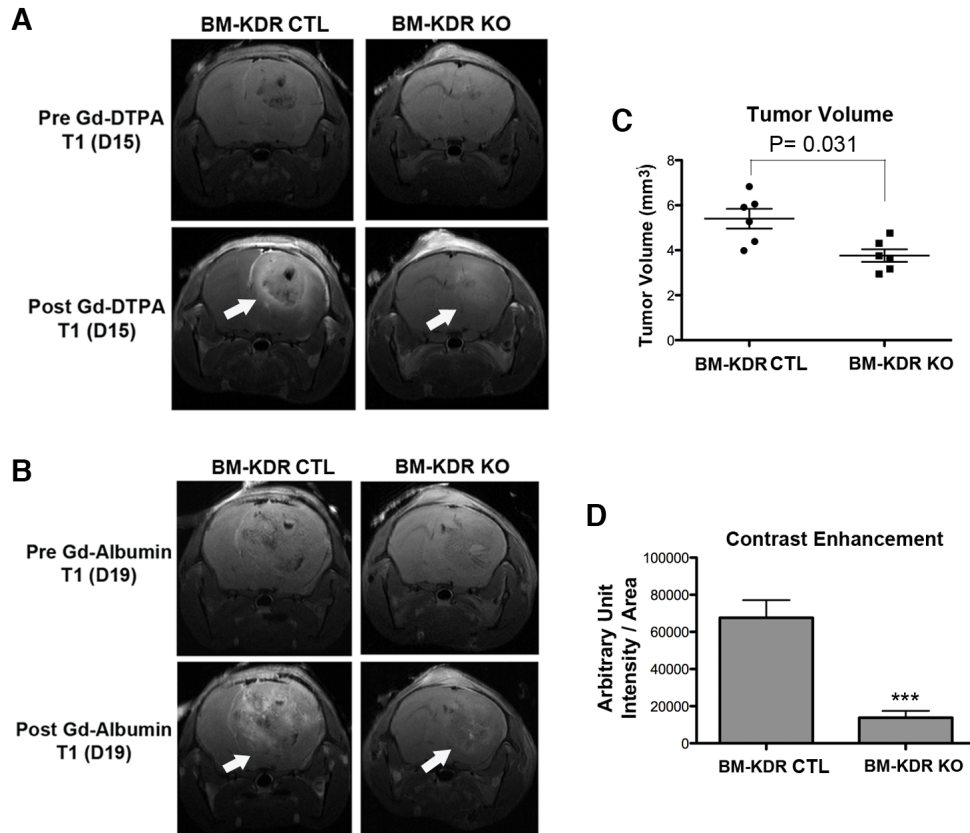
Supplementary Figure 5



Supplementary Figure 5. *KDR* knockout in BMDCs suppresses GL261 tumor growth, tumor-associated myeloid cells. (A) Chimeric C57BL/6 mice transplanted with *Rosa26Cre*^{ERT2}*KDR*^{fl/fl} and *Rosa26Cre*^{ERT2}*KDR*^{fl/+} bone marrow cells (labeled as BM-KDR KO, and BM-KDR CTL, respectively) were implanted with luciferase-labeled GL261 tumors intracranially. Tamoxifen was injected at day 3 post-implantation. Tumors were monitored by *in vivo* bioluminescence imaging. The representative image was taken at day 14 and color bar on the right represents photon intensity. The experiments have two replicates. The quantification of

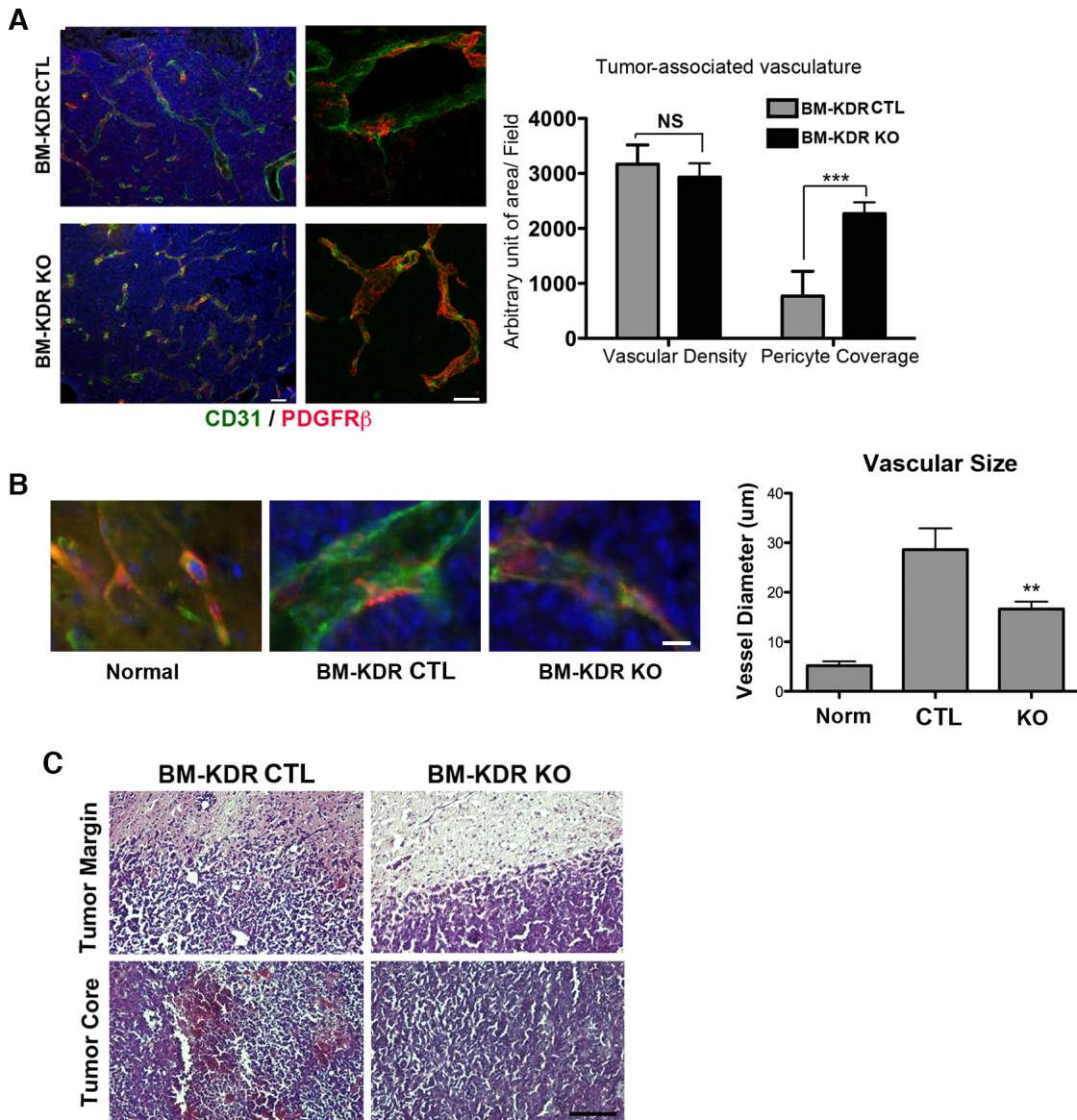
bioluminescence based tumor growth. Means \pm SD, $n=8$ $*P<0.05$ by one-way ANOVA. (B) Immunostaining of vascular basement collagen IV (green) and myeloid cells CD11b (red) in the GL261 tumors from each group. Scale bar, 20 μm . The number of CD11b cells in tumor core or tumor margin was quantified. Means \pm SD, $n=5$, Student's t-test $**P<0.01$ and $***P<0.0001$.

Supplementary Figure 6



Supplementary Figure 6. Intracranial tumors in BM-KDR KO and BM-KDR CTL groups were imaged by MRI W/O contrast dyes: Gd-DTPA (A) or Gd-Albumin (B). Quantification of tumor volumes based on T2-FLAIR MRI in BM-KDR CTL or BM-KDR KO groups. $n=5$. (C). Contrast enhancement was measured post-Gd-Albumin and were quantified by ImageJ. $P=0.031$. (D), $n=5$, Means \pm SD, Student's t-test $***P<0.001$.

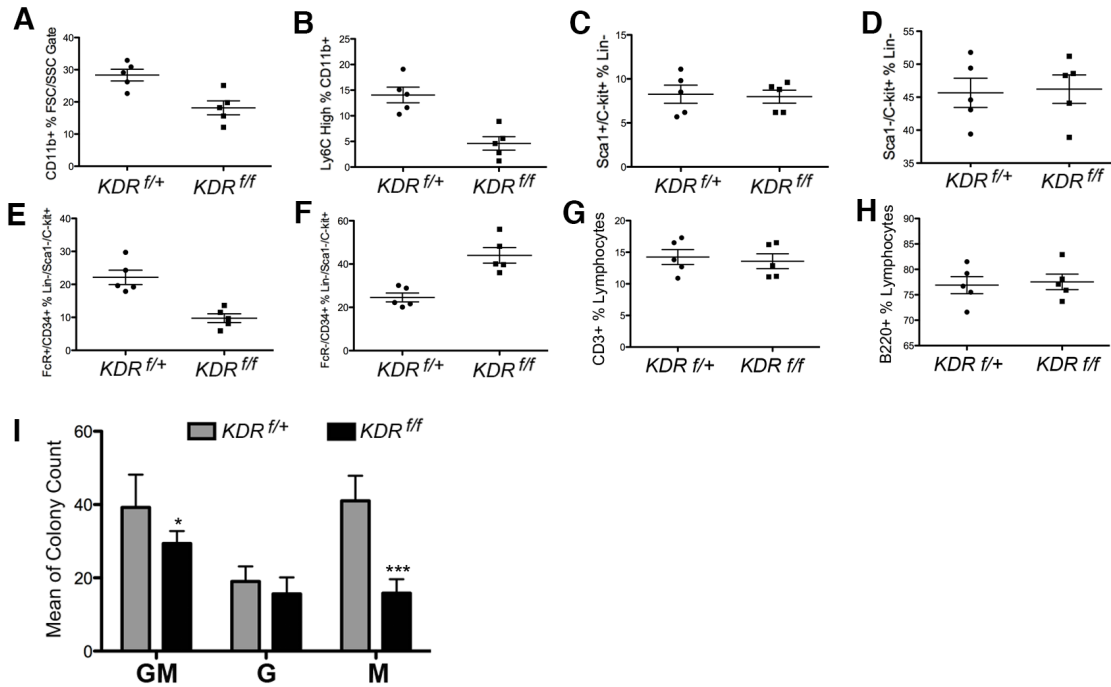
Supplementary Figure 7



Supplementary Figure 7. KDR knockout in BMDCs affects tumor vascularity. (A) Immunostaining of vascular endothelial cells (CD31) and pericytes (PDGFR β) in tumors from in BM-KDR KO and BM-KDR CTL groups. 3D reconstruction images (right) showing endothelium (green) and pericytes (red). Scale bar, 50 μm . Quantification of vascular density and pericyte coverage based area of staining. Means \pm SD, $n=5$, Student's t-test *** $P<0.0001$. (B) Magnified images of blood vessels in normal brain, tumor in BM-KDR CTL, tumor in BM-KDR KO. CD31 (green) and PDGFR β (red). Scale bar, 10 μm . Quantifications of the size of blood vessels (diameters) in each group. $n=5$, Means \pm SD, ** $P<0.01$ by one-

way ANOVA. (C) H&E staining of GL261 tumors tissue sections from each group. $n=5$, Scale bar, 50 μm .

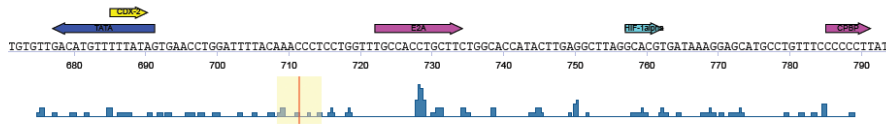
Supplementary Figure 8



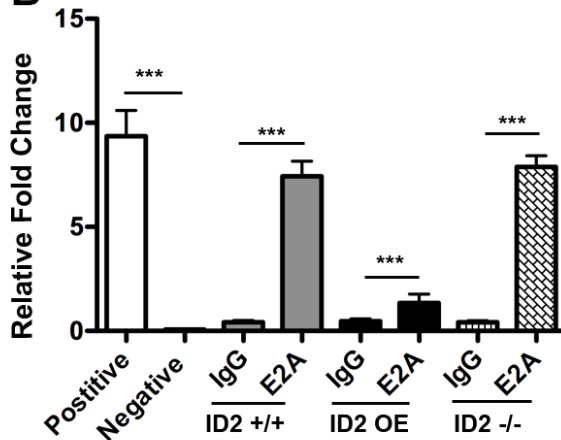
Supplementary Figure 8. Hematopoietic differentiations in BM-KDR KO mice. The quantifications on: (A) Frequency of CD11b⁺ out of total peripheral white blood cells. $P < 0.05$. (B) Frequency of Ly6C^{hi} out of total CD11b⁺ cells in peripheral. $P < 0.01$. (C) Frequency of C-kit⁺/Sca-1⁺ out of total Lin⁻ bone marrow cells. $P > 0.05$. (D) Frequency of C-kit⁺/Sca-1⁻ cells out of total Lin⁻ bone marrow cells. $P > 0.05$. (E) Frequency of FcγR⁺/CD34⁺ cells out of Lin⁻/C-kit⁺/Sca-1⁻ bone marrow cells. $P < 0.001$. (F) Frequency of FcγR⁻/CD34⁺ cells out of Lin⁻/C-kit⁻/Sca-1⁻ bone marrow cells. $P < 0.001$. T, and B cells within lymphocytes: (G) Quantification of frequency of CD3⁺ T cells in $KDR^{fl/+}$ GFP⁻ vs $KDR^{fl/fl}$ GFP⁺. $P > 0.05$. (H) Quantification of frequency of B220⁺ B cells in $KDR^{fl/+}$ GFP⁻ vs $KDR^{fl/fl}$ GFP⁺. $P > 0.05$. (a-h) $n=5$, Means \pm SD, Student's t-test. (I) Colony forming unit assay were performed on Lin⁻ Rosa26Cre^{ERT2} $KDR^{fl/fl}$ and Rosa26Cre^{ERT2} $KDR^{fl/+}$ bone marrow cells (post-tamoxifen). Macrophage (M) colonies, Macrophage/Granulocyte (GM) colonies, and Granulocyte (G) colonies were quantified. Means \pm SD, Student's t-test * $P < 0.05$, *** $P < 0.001$.

Supplementary Figure 9

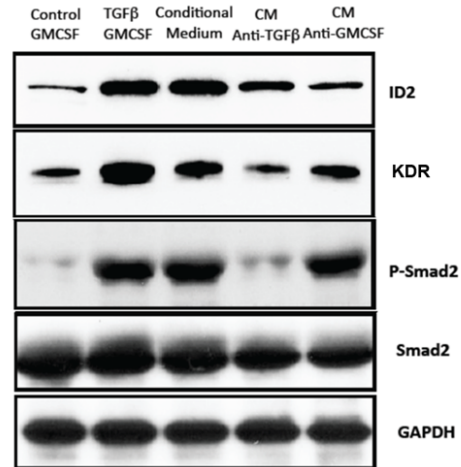
A



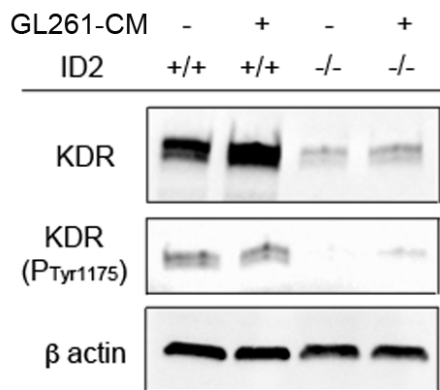
B



C



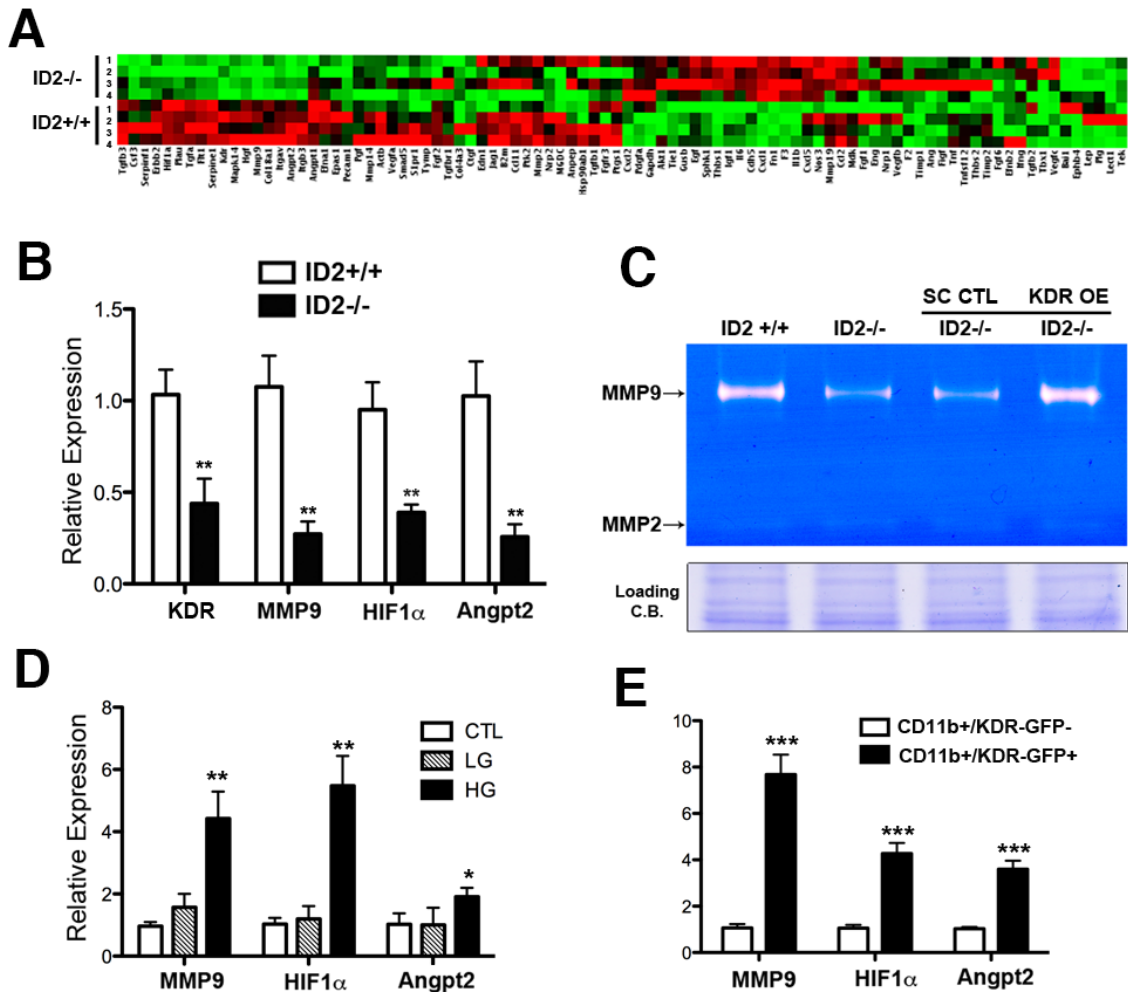
D



Supplementary Figure 9. Upstream of *KDR*. (A) The bioinformatic analysis of promoter and 5'-UTR region of *KDR* by biobase. Highlighted fragment of *KDR* promoter showed potential binding site for E2A. (B) Chromatin immunoprecipitation of E2A in ID2^{+/+} BMDCs, ID2^{+/+} with overexpression (OE) of ID2 or ID2^{-/-} BMDCs. Probe on *KDR* promoter fragments were used. Means ± SEM, ***P*<0.01, ****P*<0.0001 by one-way ANOVA. (C) Immunoblotting of KDR and ID2 on *in vitro* cultured Lin⁻ bone marrow cells treated W/WO TGF-β and GM-CSF. Phospho-smad2/smard2 indicated activation of related signaling. (D)

Immunoblotting of KDR and phosphorylated KDR ID2 on *in vitro* cultured Lin⁻ ID2^{+/+} or ID2^{-/-} bone marrow cells treated W/O GL261 conditioned medium (GL261-CM). All immunoblotting experiments have three replicates.

Supplementary Figure 10



Supplementary Figure 10. ID2/KDR affects angiogenic pathways. (A) Quantitative RT-PCR array of multiple proangiogenic and antiangiogenic factors was performed on Lin⁻ ID2^{+/+} or Lin⁻ ID2^{-/-} cells treated with TGF- β /GM-CSF. Deficient ID2 downregulates the expression level of KDR. (B) Validation of KDR, MMP9, HIF1 α , and Angiopoietin-2 (Angpt2) by quantitative RT-PCR. (C) Zymography of gelatin gels represented the enzymatic activities of MMP9/MMP2 from conditioned medium of Lin⁻ ID2^{+/+}, ID2^{-/-}, ID2^{-/-} SC CTL (transduced with scramble lentivirus), or ID2^{-/-} KDR OE (transduced with *KDR* overexpression lentivirus) HPCs pre-treated with TGF- β /GM-CSF. *n*=3. (D) The expression of

MMP9, HIF1 α , and Angpt2 in CD11b⁺ blood cells from control (CTL), low-grade (LG) and high-grade (HG) RCAS/tva mice were examined by quantitative RT-PCR. (E) The expression of MMP9, HIF1 α , and Angpt2 in CD11b⁺/KDR-GFP⁻ or CD11b⁺/KDR-GFP⁺ blood cells from high-grade glioma RCAS/tva mice. Means \pm SD, * P <0.05, ** P <0.01, *** P <0.001 by Student's t-test.